Materials Science & Engineering A 797 (2020) 140263

Contents lists available at ScienceDirect

Materials Science & Engineering A

journal homepage: http://www.elsevier.com/locate/msea

Superplastic deformation behavior of carbon nanotube reinforced 7055 Al alloy composites

S. Bi [a,b], Z.Y. Liu [a,*], B.H. Yu [a], G.N. Ma [a,b], L.H. Wu [a], B.L. Xiao [a], Z.Y. Ma [a]

[a] Institute of Metal Research, Chinese Academy of Sciences, 72 Wenhua Road, Shenyang, 110016, China
[b] University of Science and Technology of China, School of Material Science and Engineering, 72 Wenhua Road, Shenyang, 110016, China

ARTICLE INFO

Keywords:
Superplasticity
Carbon nanotubes
Aluminium matrix composites
High strain rate
Deformation mechanism

ABSTRACT

The superplastic deformation behavior of a carbon nanotube reinforced high-strength aluminium alloy matrix composite (CNT/7055Al) was investigated at temperatures ranging from 300 to 425 °C and strain rates ranging from 10^{-2} to 5 s^{-1}. A maximum elongation of 125% was observed for the as-extruded CNT/7055Al at 400 °C and a high strain rate of 5 s^{-1}. After a T6 treatment (solution and artificial aging treatment), the CNT/7055Al achieved a higher elongation of 153% at 400 °C and 5 s^{-1} due to the fewer second-phase particles. The strain rate sensitivity and activation energy were determined to be 0.2 and 171 kJ/mol, respectively. Combined with microstructural observation, it was demonstrated that the main deformation mechanism for the CNT/7055Al was lattice diffusion controlled dislocation climb. Further, it was found that CNTs played a negative role in the superplastic deformation, which could be attributed to the large aspect ratio of CNTs and strong CNT-Al interface bonding.

1. Introduction

The development of high-performance aluminium matrix composites (AMCs) is increasingly growing in order to meet the stringent requirement of aerospace industry [1–4]. Carbon nanotubes (CNTs) with ultra-high strength and modulus have attracted great research interest since their discovery in 1991 [5–8]. In the past decade, the CNT reinforced aluminium (CNT/Al) composites have been extensively studied and showed advantages over conventional particulate reinforced AMCs due to high load-transfer efficiency, good machining ability and low density [9–11]. These advantages make CNT/Al composites potential ideal structural materials in the field of aerospace.

However, CNTs enhance the strength and modulus of materials at the cost of reducing the ductility [12,13]. Choi et al. [13] produced an ultrafine-grained CNT/2024Al composite with a high yield strength of 780 MPa but a low elongation of 2%. It is found that ultrafine grain structure and constraint effect of CNTs on the matrix deformation were responsible for the brittle behavior of CNT/Al composites [14].

At elevated temperatures, dislocation motion becomes easy by climbing or cross slipping. However, CNT/Al composites still show poor ductility. Kim et al. [15] reported that a 1 vol% CNT/pure Al composite merely exhibited an elongation of less than 25% at 250 °C. A 1.5 vol% CNT/2009Al composite also exhibited poor ductility (~20%) at 300 °C [16]. This can be attributable to the strong pinning effect of CNTs on grain boundaries at elevated temperatures [17] and inappropriate deformation condition. The poor ductility at room and elevated temperatures brings considerable difficulties to the forming of CNT/Al composites and precludes their wide applications in fabrication of commercial parts.

Superplasticity refers to the ability of materials to exhibit large tensile elongations prior to failure. A wide range of complicated parts can be easily shaped by utilizing the superplastic forming [18]. In the past decades, many particulate or whisker reinforced AMCs were reported to exhibit superplasticity under appropriate temperatures and deformation rates [19–23]. For example, a 20 vol% Si_3N_{4p}/6061Al composite with a fine grain size of 1 μm could exhibit a large elongation of 626% at 560 °C and a high strain rate of 2 s^{-1} [22].

Generally, grain boundary sliding (GBS) is considered as the principal superplastic deformation mechanism for the AMCs [22,24,25], which refers to grain moving along grain boundaries. Usually, GBS could not work independently. Other mechanisms such as diffusion flow or dislocation slip assist GBS to accommodate superplastic deformation. In addition, because of introduction of reinforcements, phase interface sliding is another superplastic deformation mechanism for the AMCs, as

---

* Corresponding author.
E-mail address: zyliu@imr.ac.cn (Z.Y. Liu).

https://doi.org/10.1016/j.msea.2020.140263
Received 21 May 2020; Received in revised form 7 August 2020; Accepted 8 September 2020
Available online 9 September 2020

evidenced by the whisker debonding on fracture surfaces and dislocation-free zones adjacent to whiskers in the SiC_w/2124Al composite [14].

Two typical characteristics can be observed in superplastic deformation of the AMCs. First, the AMCs usually exhibit high strain rate superplasticity (HSRS), which is thought to be highly beneficial to the forming of materials. Fine grain structure and the presence of liquid phase are believed to be the principal contributors to the HSRS [14,26]. Second, the optimum superplastic temperature is usually close to or slightly above the solidus temperature [19]. It was demonstrated that a small amount of liquid phase was effective in relaxing stress concentration, thereby enhancing GBS or phase interface sliding processes [27,28].

To the best of our knowledge, only limited investigations have been conducted on superplastic behavior of CNT/Al composites. Huang et al. [29] firstly reported the superplastic behavior in CNT/6061Al composites. By combining hot-extrusion and hot-rolling processes, the composite with an average grain size of 580 nm showed a small elongation of 89% at 400 °C and a strain rate of 4.17×10^{-1} s^{-1}. Fan et al. [30] further refined grain structure of the composite to 300 nm by cold-rolling and improved the elongation to 150% at 375 °C and a higher strain rate of 2.08 s^{-1}. The effects of grain structure and liquid phase were discussed in these studies, but neither of them reported the role of reinforcement in the superplastic deformation since no comparison with their matrix counterparts was made.

Obviously, it is still necessary to improve the superplastic elongation of CNT/Al composites and simplify deformation process. Liu et al. [31] reported that a homogenization to as-cast 7075Al alloys by friction stir processing produced a better superplasticity for the smaller and less second-phase particles. Ma et al. [32] also suggested that reducing second-phase particle size could effectively suppress cavity nucleation during superplastic flow.

Therefore, in this study, the CNT/7055Al composites underwent a simple hot-extrusion process and were subjected to a T6 treatment (solution and artificial aging treatment) to reduce second-phase particles. The superplastic behaviors of the as-extruded and the T6 treated CNT/7055Al composites were examined. The aim of this study is to (a) achieve optimum deformation parameters of the CNT/7055Al composites, (b) improve the superplastic elongation by optimizing second phases, and (c) understand the role of CNTs in the superplastic deformation.

2. Experimental

The CNT/7055Al composite was fabricated by powder metallurgy route combined with ball-milling. 7055Al alloy (Al-8.1 wt% Zn-2.2 wt% Mg-2.2 wt% Cu) powders with an average diameter of 10 μm were ball-milled with 1 vol% multi-walled CNTs (about 10 nm in diameter, 2–5 μm in length) in an attritor at 400 rpm for 6 h [11]. Stainless steel balls (5 mm in diameter) were used as milling media. The ball-to-powder ratio was 15:1. Prior to milling, 1.6 wt% stearic acid ($CH_3(CH_2)_{16}COOH$) was added to powders as process control agent to prevent excessive cold-welding of powders [17]. The milling was conducted under an argon atmosphere and the attritor was cooled using circulating water during the process.

The milled powders were cold compacted in a cylinder die, degassed at 400 °C for 1 h and then hot-pressed at 500 °C for 1.5 h under vacuum of 10^{-1} Pa to form cylinder billet (Φ75 mm × 80 mm) [33]. The as-pressed billet was then extruded at 420 °C into bar with an extrusion ratio of 17:1. Parts of the extruded composite samples were subjected to a T6 treatment (solution treated at 470 °C for 1 h, water quenched, and aged at 120 °C for 24 h) [34]. For comparison, 7055Al alloy samples were prepared under the same process conditions and subjected to the same T6 treatment.

Tensile specimens were machined from the extruded samples along the extrusion direction. Room temperature (RT) specimens 3 mm in diameter and 15 mm in gauge length were tested on an Instron 5982 tester at the initial strain rate of 10^{-3} s^{-1}. Elevated temperature specimens 2.5 mm in gauge length, 1.4 mm in width and 1 mm in thickness were tested on an Instron 5848 tester at temperature range from 300 to 425 °C with initial strain rate range from 10^{-2} to 5 s^{-1}. 5 s^{-1} was the maximum strain rate that could be obtained in this experiment due to the limitation of the testing machine. Before elevated temperature testing, the specimens were held at the test temperature for 10 min to establish thermal equilibrium. The flow stress at each strain rate for strain-rate sensitivity calculation was taken at maximum load (UTS), where the microstructure change at this stage of hot deformation could be ignored [35].

Scanning electron microscopy (SEM, SUPRA55 and QUANTA 600) was used to characterize the second phases and cavitation. The area fraction of second phases in the samples was measured using Image-Pro Plus (IPP) 6.0 software. Transmission electron microscopy (TEM, Tecnai F20) was used to characterize the grain structure, CNT morphology and distribution. TEM specimens were cut by electrical discharge machining, ground to a thickness of 60 μm, punched to disks with a diameter of 3 mm, then dimpled to a minimum thickness of 20 μm and finally ion-beam thinned by a Gatan Model 691 ion milling system at 6° and 4.5 keV.

3. Results

3.1. Microstructures and RT mechanical properties of CNT/7055Al

The grain structures of the as-extruded and T6 treated CNT/7055Al are respectively shown in Fig. 1(a) and (b). After the statistical measurement of about 70 grains in TEM images, the average grain sizes (average value of length and width of a grain) of the as-extruded and T6 treated samples were determined to be 308 ± 96 nm and 330 ± 127 nm, respectively. The enlarged TEM images indicate that the grains in the both composites were in irregular shape (Fig. 1(c) and (d)). The distribution of CNTs in the composite is shown in Fig. 1(e). It can be seen that CNTs were uniformly dispersed and were approximately aligned along the extrusion direction in the Al matrix. The average length of CNTs was estimated to be ~100 nm.

The engineering stress-strain curves of the T6 treated CNT/7055Al and 7055Al alloy at RT are shown in Fig. 2. The composite exhibited a high tensile strength of 760 MPa with 60 MPa enhancement over the 7055Al alloy, proving that the CNT/Al composites based on 7xxx series Al alloys had strength advantage over those based on pure Al, 2xxx or 6xxx series Al alloys prepared using the similar route [10,17,36–38].

3.2. Phase variation at RT and elevated temperatures

Fig. 3 shows second phases in the as-extruded and T6 treated CNT/7055Al at RT and 400 °C held for 15 min (this time is approximately equivalent to the total time of holding and testing time for superplastic tension). At RT, a large number of second phases with sizes of 0.2–1 μm were densely distributed in the Al matrix for the as-extruded sample (Fig. 3(a)). These second phases, identified from energy spectrum, were mainly composed of $MgZn_2$ phase which was a common precipitate in 7xxx series Al alloys [39,40]. The representative energy spectrum data are shown in the insets in Fig. 3. For the T6 treated sample (Fig. 3(b)), the second phases were much less and they were identified as $MgZn_2$ phase (small, marked in rectangle) and impurity phase Al_7Cu_2Fe (large and bright, marked in arrows) [41,42].

After holding at 400 °C for 15 min, as shown in Fig. 3(c) and (d), the number of second phases in the as-extruded sample decreased dramatically while those in the T6 treated sample decreased slightly. Statistics indicated that second phases in Fig. 3(c) and (d) accounted for 4.9% and 2.6% in area fraction, respectively, based on IPP software. This suggests that the as-extruded sample had more particles than the T6 treated one during tension at 400 °C.

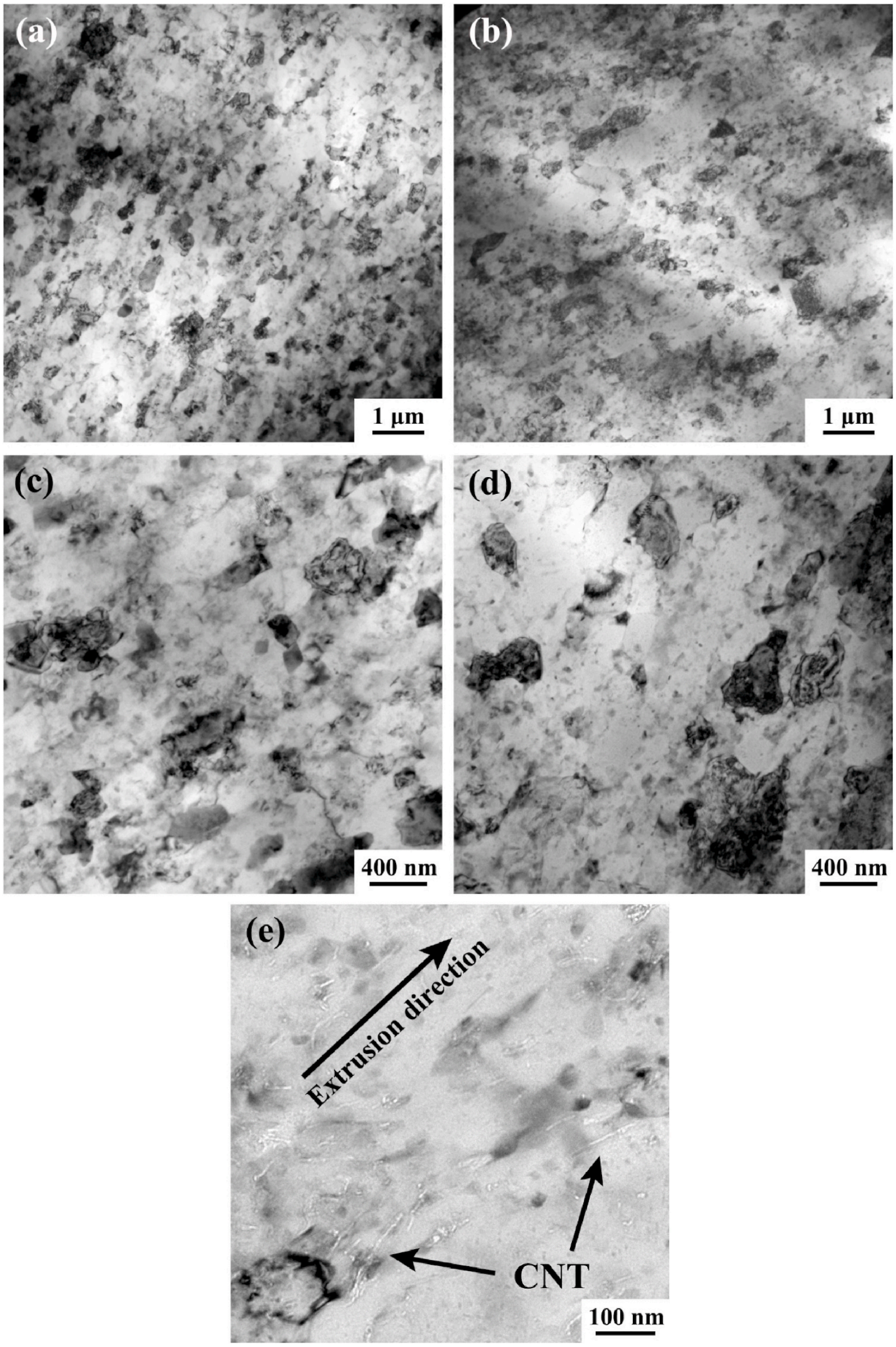

Fig. 1. TEM images showing grain structures of (a, c) as-extruded and (b,d) T6 treated CNT/7055Al, and (e) distribution of CNTs.

3.3. Superplastic behavior of CNT/7055Al

3.3.1. True stress-strain curves

Fig. 4 shows the true stress-strain curves of the T6 treated 7055Al and CNT/7055Al samples at 400 °C with strain rates ranging from 10^{-2} to 5 s^{-1}. The stress-strain curves of 7055Al and CNT/7055Al exhibited the same trend irrespective of strain rates, indicating the same deformation mechanism for them. Of all the curves, the flow stresses reached a maximum value at first and then decreased slowly until the occurrence of localized necking. These curves belonged to a “nearly steady-state” curve type. Similar curves were observed in the mechanical alloyed Al-8 wt% Ti alloy [43].

3.3.2. Elongation at different parameters

Fig. 5 shows the variations of elongation with the initial strain rate at different testing temperatures for 7055Al and CNT/7055Al. For all samples, the optimum strain rate for maximum elongation increased with increasing temperature. The maximum elongations were respectively obtained at 400 °C at 5 s^{-1} and at 400 °C at 3 s^{-1} for the composite samples and the alloy samples. The maximum elongations of the T6 treated 7055Al, as-extruded CNT/7055Al and T6 treated CNT/7055Al were 407%, 125% and 153%, respectively. When the temperature was higher than 400 °C, the elongations decreased for all samples. The elongation data obtained from the T6 treated CNT/7055Al are equivalent to those from the CNT/6061Al (150%) reported by Fan et al. [30], but the material fabrication process in this study was simpler. The

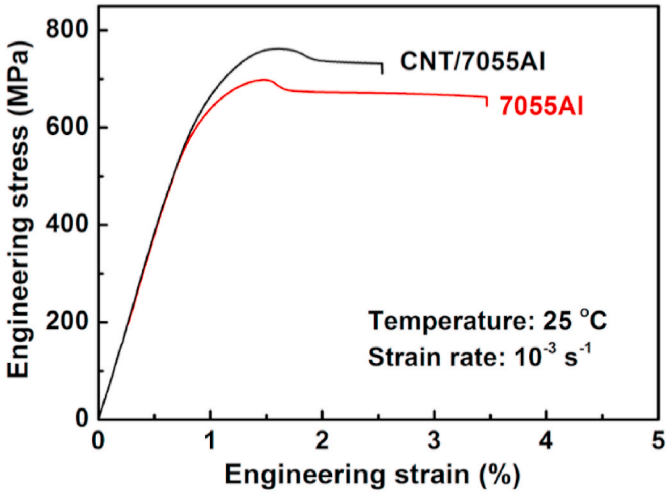

Fig. 2. Engineering stress-strain curves of T6 treated CNT/7055Al and 7055Al alloy.

elongation at 400 °C for CNT/7055Al might be further improved if larger strain rates were allowed, according to the change trend of elongation (Fig. 5(c)).

3.3.3. *Flow stress*

Fig. 6 shows the variations of flow stress with initial strain rate for 7055Al and CNT/7055Al. The slope of the curve stands for the strain-rate sensitivity m ($=\frac{\partial(lg\sigma)}{\partial(lg\dot{\varepsilon})}$, where σ is the flow stress and $\dot{\varepsilon}$ is the strain rate). Generally, a high m value indicates a large elongation for superplastic materials. As shown in Fig. 6, at lower strain rates ($<10^{-1}$ s^{-1}), very low m values (<0.1) were observed for all samples. With increasing the strain rate, the m value increased. The maximum m value was obtained for either the alloy samples or the composite samples at the optimum temperature of 400 °C and the strain rate larger than 3×10^{-1} s^{-1}, which was in accordance with the maximum elongations. It is noted that the optimum elongation of the alloy samples was higher than 400%, but the m value was much lower than 0.33, indicating the existence of threshold stress in these materials [43,44].

3.4. *Observation of cavitation*

Fig. 7 shows the lateral surfaces of the polished CNT/7055Al samples after tension at 400 °C and 5 s^{-1}. The images with low magnifications in

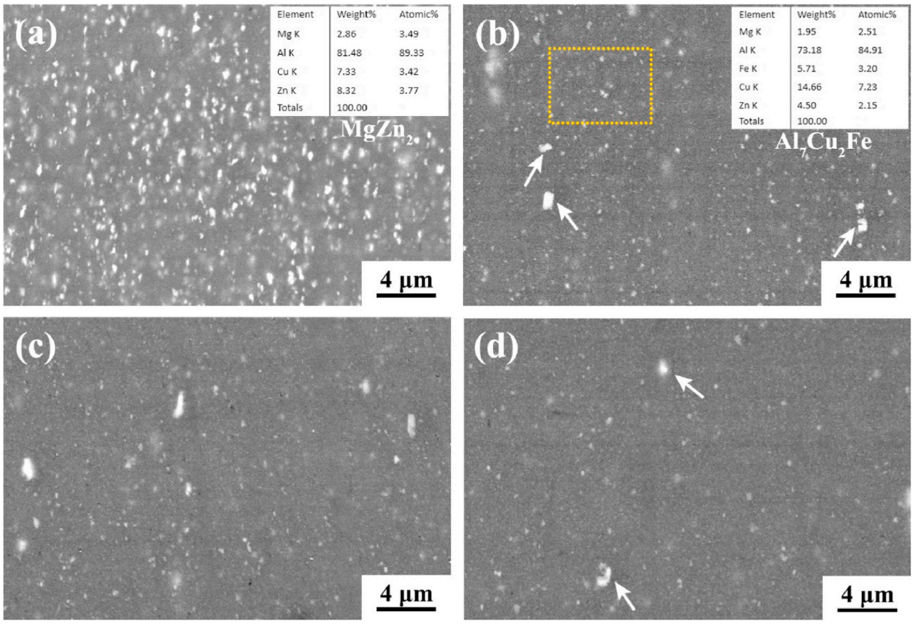

Element	Weight%	Atomic%
Mg K	2.86	3.49
Al K	81.48	89.33
Cu K	7.33	3.42
Zn K	8.32	3.77
Totals	100.00	

Element	Weight%	Atomic%
Mg K	1.95	2.51
Al K	73.18	84.91
Fe K	5.71	3.20
Cu K	14.66	7.23
Zn K	4.50	2.15
Totals	100.00	

Fig. 3. Back scattered SEM images of (a) as-extruded and (b) T6 treated CNT/7055Al at RT; (c) as-extruded and (d) T6 treated CNT/7055Al held at 400 °C for 15 min (the rectangle denotes $MgZn_2$ phases, the arrows denote Al_7Cu_2Fe phases).

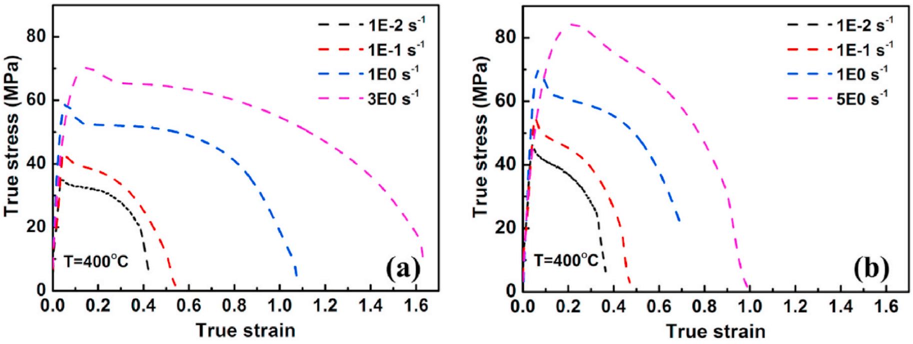

Fig. 4. Plots of true stress-true strain curves at 400 °C at different initial strain rates for T6 treated (a) 7055Al and (b) CNT/7055Al.

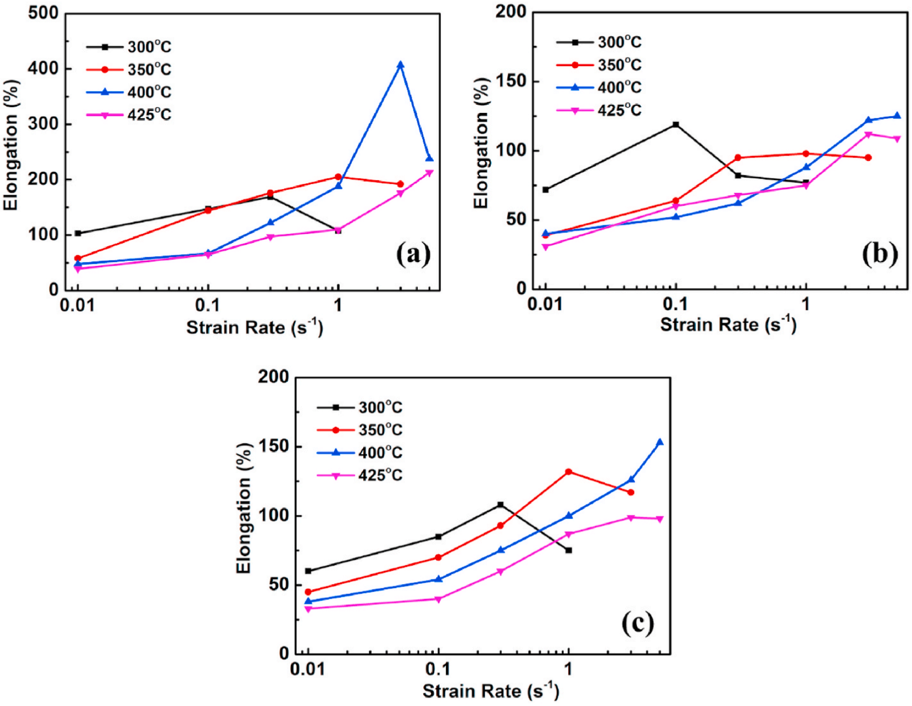

Fig. 5. Variations of elongation with initial strain rate at various testing temperatures: (a) T6 treated 7055Al, (b) as-extruded CNT/7055Al and (c) T6 treated CNT/7055Al.

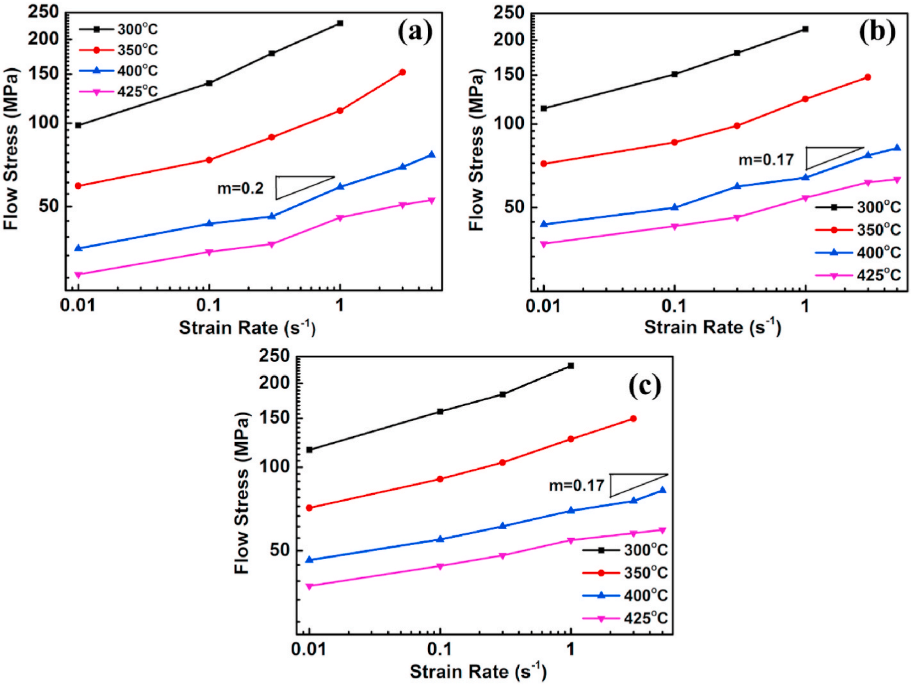

Fig. 6. Variations of flow stress with initial stain rate for (a) T6 treated 7055Al, (b) as-extruded CNT/7055Al and (c) T6 treated CNT/7055Al.

Fig. 7(a) and (b) demonstrate that the cavities for both composite samples were concentrated near the fracture tips and the cavities in the as-extruded sample were larger than those in the T6 treated sample. These cavities were in the typical “V” shape with sizes of several micrometers (marked by arrows). “V”-shaped cavities are usually formed under high stress condition and caused by stress concentration [45]. From the magnified images (Fig. 7(c) and (d)), granular structure was observed on the surfaces of both samples, implying the GBS during superplastic deformation. Similar structure was also observed in the superplastic deformation of mechanically alloyed materials [43,44].

3.5. Determination of threshold stress

The threshold stress σ_0 is determined from a linear extrapolation of the superplastic data to zero strain rate by plotting $\dot{\varepsilon}^m$ against σ on linear axes. This method requires the introduction of assumed m values and the

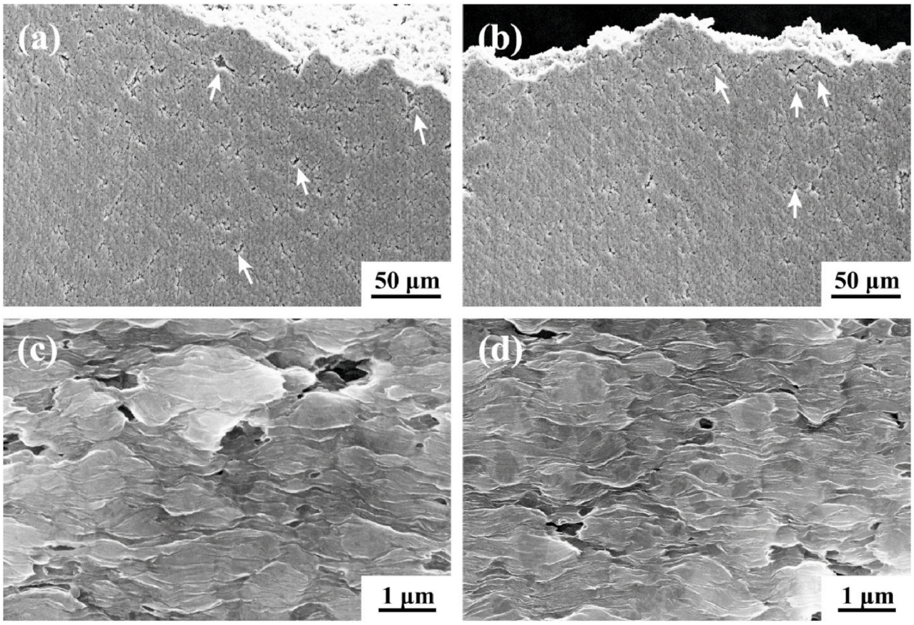

Fig. 7. SEM images of lateral surfaces of tensile samples tested at 400 °C and 5 s^{-1}: (a, c) as-extruded CNT/7055Al and (b, d) T6 treated CNT/7055Al (the arrows denote the "V"-shaped cavities).

best value for *m* is determined from the best linear fit of the data. The calculated values of *m* in various materials are shown in Fig. 8. The results indicate that the threshold stresses existed in the alloy and composites. With the increase of assumed *m* values, the threshold stresses increase. For the alloy, the *m* value was determined to be 0.33. However, for the composites, both the *m* values were determined to be 0.2. This indicates the dominant deformation mechanisms for 7055Al and CNT/7055Al were related to dislocation motion rather than GBS ($m = 0.5$).

3.6. Fracture surface examination

The fractographs of the T6 treated CNT/7055Al after tension at RT and 400 °C are shown in Fig. 9(a) and (b), respectively. For the RT fracture surface, a large number of CNTs (shown in white arrows) were pulled out and distributed at the bottom of dimples. The dimples were small and shallow, which was in accordance with the low elongation at RT. At elevated temperature, the dimples on the fracture surface became larger, indicating that large deformation happened at grain interiors. Several pulled-out CNTs with random orientations were observed. And

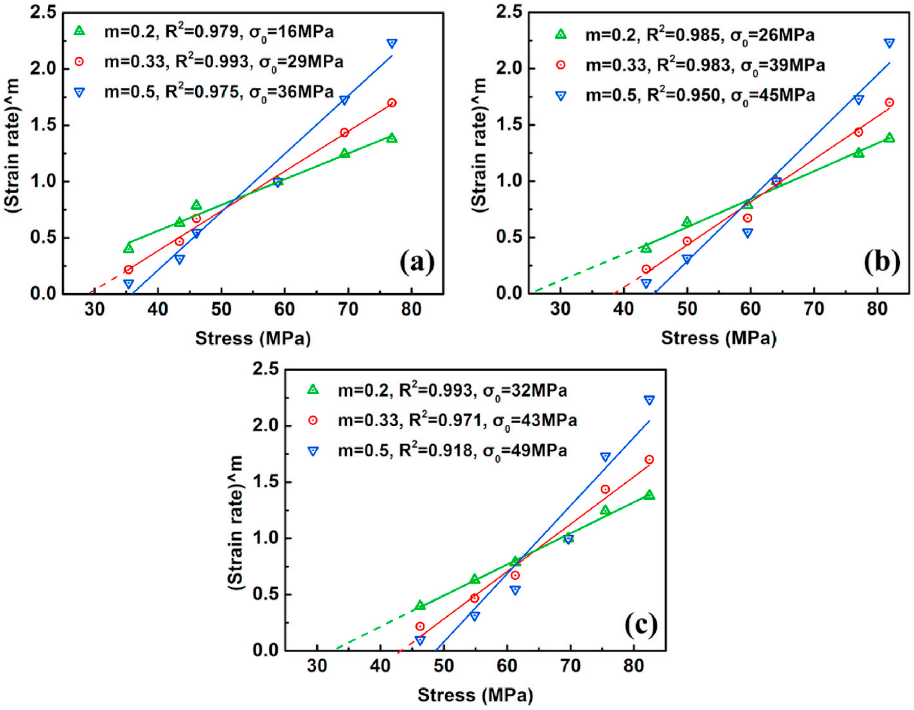

Fig. 8. Determination of threshold stress at 400 °C using different assumed *m* values for (a) T6 treated 7055Al, (b) as-extruded CNT/7055Al and (c) T6 treated CNT/7055Al.

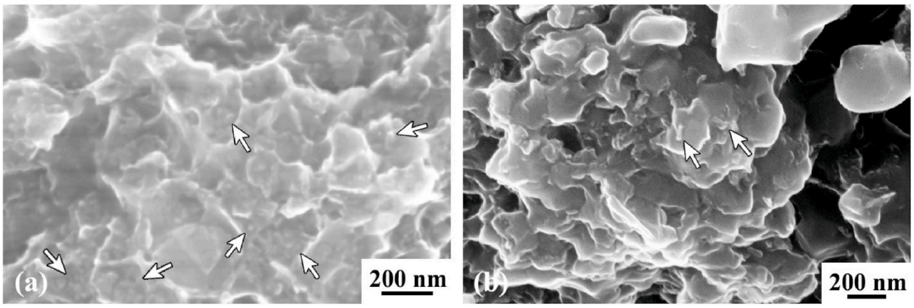

Fig. 9. Fractographs of T6 treated CNT/7055Al samples tested (a) at RT and 10^{-3} s^{-1} and (b) at 400 °C and 5 s^{-1} (the arrows denote CNTs).

the length of pulled-out CNTs was larger than that on the RT fracture surface, which suggests the occurrence of the phase interface sliding between CNTs and the Al matrix during deformation process for the T6 treated CNT/7055Al.

3.7. *Microstructure after superplastic deformation*

Fig. 10 shows the microstructure of T6 treated CNT/7055Al deformed at 400 °C and 5 s^{-1}. The grains after superplastic deformation were obviously elongated, as shown in Fig. 10(a) (marked by yellow dot line). Some grains were even up to 1 μm in length compared to the grains with average length of less than 500 nm before deformation. This microstructure change indicates that grains deformed along the tensile direction during testing process, supporting the observation on the fracture surfaces (Fig. 9(b)). A close examination at the grain interior is shown in Fig. 10(b). A high density of dislocations and substructures were observed. This indicates that a higher density of dislocations was generated by plastic deformation in CNT/7055Al. It demonstrates that dislocations played a significant role in accommodating superplastic deformation.

4. Discussion

4.1. *Deformation mechanism for CNT/7055Al*

The deformation mechanism for superplastic materials is closely associated with activation energy. The activation energy can be obtained by the following equation which is derived from the well-established strain rate-stress equation [46].

$$Q = R\frac{\partial \ln\left[(\sigma-\sigma_0)^n/G^{n-1}T\right]}{\partial(1/T)} \tag{1}$$

where Q is the activation energy, σ is the flow stress, σ_0 is the threshold stress, n *is* the stress exponent (reciprocal to the strain rate sensitivity m, i.e. $m = 1/n$), T is the temperature and G is the shear modulus. G is dependent on the temperature and can be described as [47]:

$$G = 4.2535 \times 10^4 - 14T \tag{2}$$

Fig. 11 shows the plot of $R\ \ln[(\sigma-\sigma_0)^n/G^{n-1}T]$ versus $1/T$ at a strain rate of 10^{-1} s^{-1} with $m = 0.2$ for the T6 treated CNT/7055Al. The activation energy for the T6 treated CNT/7055Al was determined to be 171 kJ/mol. This value is higher than the activation energy for lattice self-diffusion in Al (142 kJ/mol) [29]. Similar results were also observed in other superplastic AMCs [19,48]. The high activation energy for the AMCs was attributable to the introduction of reinforcements. Firstly, interfacial sliding between reinforcements and matrix needs diffusion process to accommodate [49]. Secondly, the load transfer from the matrix to the reinforcements depending on temperature also makes a contribution to the activation energy, as demonstrated by Li et al. [50].

Based on aforementioned experimental observations and calculation ($m = 0.2$ and $Q = 171$ kJ/mol), three possible deformation mechanisms were responsible for the superplasticity of CNT/7055Al. The first mechanism was interfacial sliding, which was common in the deformation of the AMCs. However, this mechanism was not dominant for the CNT/7055Al because no many pulled-out CNTs were observed after deformation [14]. Also, the volume fraction of CNTs was not high enough to support such a large deformation.

The second mechanism was GBS proved by the granular structure on lateral surface of the deformed samples (Fig. 7(c) and (d)). However, GBS was not the primary mechanism due to the following two reasons. On one hand, the volume fraction of cavities at the fracture tip was small, indicating that only part of the high-angle grain boundaries could slide during deformation [44]. On the other hand, the flow stresses of CNT/7055Al were very high as compared to the typical superplastic

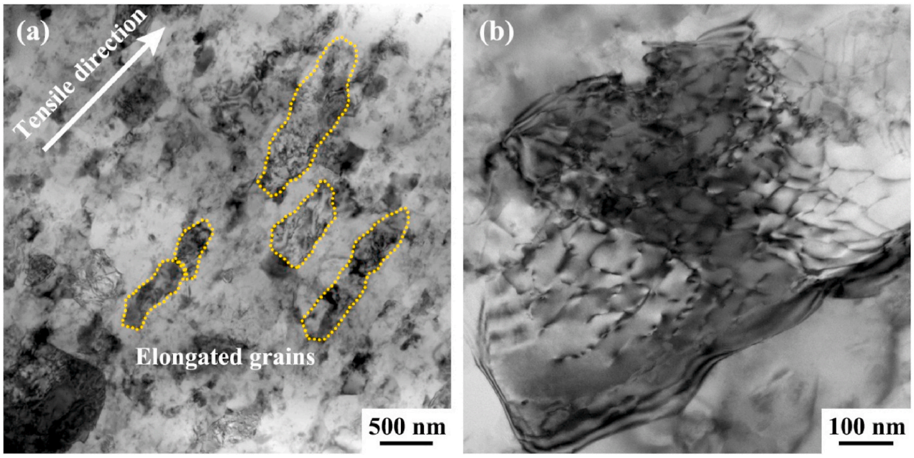

Fig. 10. Microstructure of T6 treated CNT/7055Al after tension at 400 °C and 5 s^{-1}: (a) grain structure and (b) dislocations at grain interior.

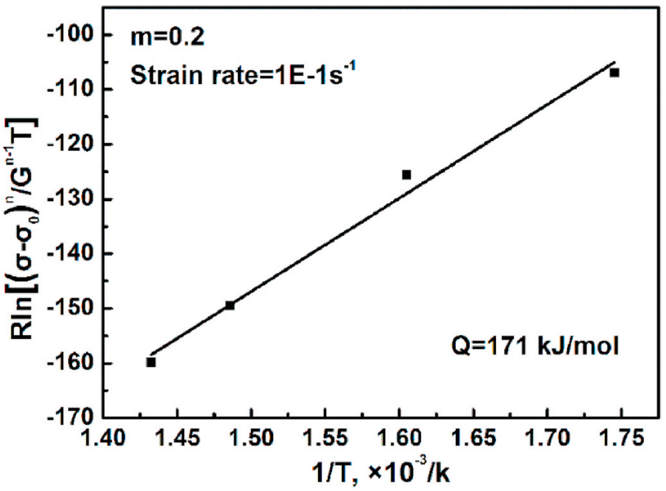

Fig. 11. Plot of $R\ln[(\sigma-\sigma_0)^n/G^{n-1}T]$ versus $1/T$ at a strain rate of 10^{-1} s^{-1} with $m = 0.2$ for T6 treated CNT/7055Al.

7055Al alloys [51,52], indicating that the intragranular deformation (dislocation motion, etc.) played a main role in the superplastic deformation [44].

The third mechanism was the lattice diffusion controlled dislocation climb. The m value of 0.2 indicated the operation of lattice diffusion controlled dislocation climb mechanism [18,53], which could be evidenced by the high density of dislocations in the grain interior after deformation. In addition, other evidences such as the activation energy close to that for the self-lattice diffusion in Al, elongated grains and dimples after deformation also supported this deformation mechanism.

4.2. The effect of second phases on superplastic deformation

As described above, the T6 treated CNT/7055Al exhibited a higher elongation (153%) than the as-extruded one (125%). The superplastic elongation of the CNT/7055Al was improved by optimizing second-phase particles. As discussed above, the superplastic deformation mechanism of the CNT/7055Al was associated with dislocation motion. The T6 treated CNT/7055Al had fewer second-phase particles, which made dislocations easy to pass by during deformation, resulting in the higher elongation. In addition, once the superplastic deformation could not be accommodated by dislocation climb or diffusion flow, cavity initiation would occur. The second-phase particles were the stress concentration locations, where cavities easily nucleated [31]. Therefore, cavities with larger size were observed on the surface of the deformed samples for the as-extruded CNT/7055Al than that for the T6 treated one, which led to the premature fracture of the as-extruded composite. The above analysis indicates that optimizing second-phase particles through a T6 treatment is a strategy to improve the superplasticity of the CNT/Al composites.

4.3. The role of CNTs during superplastic deformation

As shown in Fig. 5, the superplastic elongation of the T6 treated CNT/7055Al was much lower than that of the T6 treated 7055Al alloy. This suggested that CNTs played a negative role in the superplastic deformation. Low superplastic elongation was also observed in other CNT/Al composites [29,30]. This could result from the following reasons. Firstly, most of the CNTs were distributed at grain boundaries, which greatly limited the GBS mechanism. Secondly, interfacial sliding failed to play a major role in the deformation. Although some of phase interfaces that facilitated superplastic flow were created by introduction of CNTs, only a few pulled-out CNTs could be seen after deformation. This might be due to the strong interfacial bonding between Al matrix and CNTs [17]. Thirdly, dislocations played an important role in the superplastic deformation. CNTs inside grains probably hindered dislocation motion during the deformation. CNTs had large aspect ratios, which made CNTs cross multiple glide planes, thereby increasing the interaction between CNTs and dislocations. The above reasons led to the lower superplastic elongation of the CNT/7055Al composite than that of the 7055Al alloy.

5. Conclusions

The superplastic behavior of CNT/7055Al composites fabricated by ball-milling and powder metallurgy route was investigated under different temperatures and strain rates. The deformation mechanism and the factors affecting deformation were discussed. The following conclusions can be drawn:

1) By reducing the second-phase particles via a T6 treatment (solution and artificial aging treatment), the superplastic elongation of the CNT/7055Al was improved. The T6 treated and the as-extruded CNT/7055Al both achieved their highest superplastic elongations at 400 °C and 5 s^{-1}, with maximum elongations of 153% and 125%, respectively.
2) The activation energy and m value for the T6 treated CNT/7055Al were determined to be 171 kJ/mol and 0.2, respectively. Combined with the microstructural observation of plenty of dislocations in the deformed grains, lattice diffusion controlled dislocation climb was determined to be the main deformation mechanism for the CNT/7055Al. Grain boundary sliding and interfacial sliding played minor roles in the deformation.
3) CNTs played a negative role in the superplastic deformation due to the hindrance of CNTs to dislocation motion and grain boundary sliding. The large aspect ratio of CNTs and strong CNT/Al interface bonding might be the reasons for the low superplastic elongation in CNT/7055Al composites.

CRediT authorship contribution statement

S. Bi: All authors contribute substantially to the paper, Formal analysis, helped to analyze the. **Z.Y. Liu:** Formal analysis, Data curation, (first author) carried out the data collection, data analysis and manuscript writing. **B.H. Yu:** revised the manuscript. **G.N. Ma:** Formal analysis. **L.H. Wu:** Formal analysis, helped to analyze the microstructure. **B.L. Xiao:** Funding acquisition. **Z.Y. Ma:** Funding acquisition, designed the experiment and provided the fund.

Declaration of competing interest

The authors declare that they have no known competing financial interests or personal relationships that could have appeared to influence the work reported in this paper.

Acknowledgements

The authors gratefully acknowledge the support of (a) Key Research Program of Frontier Sciences, CAS (No. QYZDJ-SSW-JSC015); National Key R&D Program of China (No. 2017YFB0703104); The project of manned spaceflight (No. 040103), (b) the National Natural Science Foundation of China (No. 51931009, No. 51871215), (c) the Youth Innovation Promotion Association CAS (2020197).

References

[1] K. Ma, X. Zhang, D. Wang, Q. Wang, Z. Liu, B. Xiao, Z. Ma, Optimization and simulation of deformation parameters of SiC/2009Al composites, Acta Metall. Sin. 55 (2019) 1329–1337, https://doi.org/10.11900/0412.1961.2019.00020.

[2] G. Ma, D. Wang, Z. Liu, S. Bi, Y. Zan, B. Xiao, Z. Ma, Effect of hot pressing temperature on microstructure and tensile properties of SiC/Al-Zn-Mg-Cu

composites, Acta Metall. Sin. 55 (2019) 1319–1328, https://doi.org/10.11900/0412.1961.2018.00523.

[3] J.F. Zhang, X.X. Zhang, Q.Z. Wang, B.L. Xiao, Z.Y. Ma, Simulations of deformation and damage processes of SiCp/Al composites during tension, J. Mater. Sci. Technol. 34 (2018) 627–634, https://doi.org/10.1016/j.jmst.2017.09.005.

[4] Z.Y. Liu, L.H. Wang, Y.N. Zan, W.G. Wang, B.L. Xiao, D. Wang, et al., Enhancing strengthening efficiency of graphene nano-sheets in aluminum matrix composite by improving interface bonding, Composites Part B 199 (2020) 108268, https://doi.org/10.1016/j.compositesb.2020.108268.

[5] S. Iijima, Helical microtubules of graphitic carbon, Nature 354 (1991) 56–58, https://doi.org/10.1038/354056a0.

[6] D. Qian, G.J. Wagner, W.K. Liu, M.-F. Yu, R.S. Ruoff, Mechanics of carbon nanotubes, Appl. Mech. Rev. 55 (2002) 495, https://doi.org/10.1115/1.1490129.

[7] J.P. Salvetat-Delmotte, A. Rubio, Mechanical properties of carbon nanotubes: a fiber digest for beginners, Carbon 40 (2002) 1729–1734, https://doi.org/10.1016/S0008-6223(02)00012-X.

[8] X. Liu, J. Li, J. Sha, E. Liu, Q. Li, C. He, C. Shi, N. Zhao, In-situ synthesis of graphene nanosheets coated copper for preparing reinforced aluminum matrix composites, Mater. Sci. Eng., A 709 (2018) 65–71, https://doi.org/10.1016/j.msea.2017.10.030.

[9] Z.Y. Liu, B.L. Xiao, W.G. Wang, Z.Y. Ma, Developing high-performance aluminum matrix composites with directionally aligned carbon nanotubes by combining friction stir processing and subsequent rolling, Carbon 62 (2013) 35–42, https://doi.org/10.1016/j.carbon.2013.05.049.

[10] H. Choi, J. Shin, B. Min, J. Park, D. Bae, Reinforcing effects of carbon nanotubes in structural aluminum matrix nanocomposites, J. Mater. Res. 24 (2009) 2610–2616, https://doi.org/10.1557/jmr.2009.0318.

[11] Z.Y. Liu, K. Ma, G.H. Fan, K. Zhao, J.F. Zhang, B.L. Xiao, Z.Y. Ma, Enhancement of the strength-ductility relationship for carbon nanotube/Al–Cu–Mg nanocomposites by material parameter optimisation, Carbon 157 (2020) 602–613, https://doi.org/10.1016/j.carbon.2019.10.080.

[12] C.N. He, N.Q. Zhao, C.S. Shi, S.Z. Song, Mechanical properties and microstructures of carbon nanotube-reinforced Al matrix composite fabricated by in situ chemical vapor deposition, J. Alloys Compd. 487 (2009) 258–262, https://doi.org/10.1016/j.jallcom.2009.07.099.

[13] H.J. Choi, B.H. Min, J.H. Shin, D.H. Bae, Strengthening in nanostructured 2024 aluminum alloy and its composites containing carbon nanotubes, Composites Part A 42 (2011) 1438–1444, https://doi.org/10.1016/j.compositesa.2011.06.008.

[14] T.G. Nieh, J. Wadsworth, High-strain-rate superplasticity in aluminum matrix composites, Mater. Sci. Eng., A 147 (1991) 129–142, https://doi.org/10.1016/0921-5093(91)90839-F.

[15] W.J. Kim, S.H. Lee, High-temperature deformation behavior of carbon nanotube (CNT)-reinforced aluminum composites and prediction of their high-temperature strength, Composites Part A 67 (2014) 308–315, https://doi.org/10.1016/j.compositesa.2014.09.008.

[16] Z.Y. Liu, B.L. Xiao, W.G. Wang, Z.Y. Ma, Elevated temperature tensile properties and thermal expansion of CNT/2009Al composites, Compos. Sci. Technol. 72 (2012) 1826–1833, https://doi.org/10.1016/j.compscitech.2012.07.021.

[17] Z.Y. Liu, B.L. Xiao, W.G. Wang, Z.Y. Ma, Modelling of carbon nanotube dispersion and strengthening mechanisms in Al matrix composites prepared by high energy ball milling-powder metallurgy method, Composites Part A 94 (2017) 189–198, https://doi.org/10.1016/j.compositesa.2016.11.029.

[18] O.D. Sherby, J. Wadsworth, Superplasticity-Recent advances and future directions, Prog. Mater. Sci. 33 (1989) 169–221, https://doi.org/10.1016/0079-6425(89)90004-2.

[19] B.Q. Han, K.C. Chan, High-strain-rate superplasticity of an Al6061/SiC_w composite, Scripta Mater. 36 (1997) 593–598, https://doi.org/10.1016/S1359-6462(96)00426-5.

[20] M.W. Mahoney, A.K. Ghosh, Superplasticity in a high strength powder aluminum alloy with and without SiC reinforcement, Metall. Mater. Trans. 18 (1987) 653–661, https://doi.org/10.1007/BF02649481.

[21] M. Mabuchi, K. Higashi, S. Tanimura, T. Imai, K. Kubo, Superplastic-like behavior in as-extruded Al-Zn-Mg alloy matrix composites reinforced with Si3N4 whiskers, Scripta Mater. 25 (1991) 1675–1680, https://doi.org/10.1016/0956-716X(91)90473-E.

[22] M. Mabuchi, K. Higashi, Y. Okada, S. Tanimura, T. Imai, K. Kubo, Very high strain-rate superplasticity in a particulate Si_3N_4/6061 aluminum composite, Scripta Mater. 25 (1991) 2517–2522, https://doi.org/10.1016/0956-716X(91)90060-E.

[23] T.G. Nieh, C.A. Henshall, J. Wadsworth, Superplasticity at high strain rates in a SiC reinforced Al alloy, Scripta Mater. 18 (1984) 1405–1408, https://doi.org/10.1016/0036-9748(84)90374-0.

[24] R.S. Mishira, T.R. Bieler, A.K. Mukherjee, Superplasticity in powder metallurgy aluminum alloys and composites, Acta Mater. 43 (1995) 877–891, https://doi.org/10.1016/0956-7151(94)00323-A.

[25] M. Mabuchi, T. Imai, K. Kubo, K. Higashi, Y. Okada, S. Tanimura, Superplasticity in as-extruded Si_3N_{4w}/6061 aluminum composites processed at a ratio of 100: 1, Mater. Lett. 11 (1991), https://doi.org/10.1016/0167-577X(91)90129-T.

[26] G.M. Pharr, M.F. Ashby, On creep enhanced by a liquid phase, Acta Mater. 31 (1983) 129–138, https://doi.org/10.1016/0001-6160(83)90072-X.

[27] M. Mabuchi, K. Higashi, T.G. Langdon, An investigation of the role of a liquid phase in a Al-Cu-Mg metal matrix composites exhibiting high strain rate superplasticity, Acta Mater. 42 (1994) 1739–1745, https://doi.org/10.1016/0956-7151(94)90384-0.

[28] K. Higashi, Deformation mechanisms of positive exponent superplasticity in advanced aluminum alloys with nano or near-nano scale grained structures, Mater. Sci. Forum 170 (1994) 131–140. https://doi.org/10.4028/www.scientific.net/MSF.170-172.131.

[29] H. Huang, G. Fan, Z. Tan, D.-B. Xiong, Q. Guo, C. Guo, Z. Li, D. Zhang, Superplastic behavior of carbon nanotube reinforced aluminum composites fabricated by flake powder metallurgy, Mater. Sci. Eng., A 699 (2017) 55–61, https://doi.org/10.1016/j.msea.2017.05.074.

[30] G. Fan, H. Huang, Z. Tan, D. Xiong, Q. Guo, M. Naito, Z. Li, D. Zhang, Grain refinement and superplastic behavior of carbon nanotube reinforced aluminum alloy composite processed by cold rolling, Mater. Sci. Eng., A 708 (2017) 537–543, https://doi.org/10.1016/j.msea.2017.10.031.

[31] F.C. Liu, Z.Y. Ma, Achieving high strain rate superplasticity in cast 7075Al alloy via friction stir processing, J. Mater. Sci. 44 (2009) 2647–2655, https://doi.org/10.1007/s10853-009-3346-6.

[32] Z.Y. Ma, R.S. Mishra, Cavitation in superplastic 7075Al alloys prepared via friction stir processing, Acta Mater. 51 (2003) 3551–3569, https://doi.org/10.1016/S1359-6454(03)00173-3.

[33] Z. Zhang, S. Dallek, R. Vogt, Y. Li, T.D. Topping, Y. Zhou, J.M. Schoenung, E. J. Lavernia, Degassing behavior of nanostructured Al and its composites, Metall. Mater. Trans. 41 (2009) 532–541, https://doi.org/10.1007/s11661-009-0089-6.

[34] J. Chen, L. Zhen, S. Yang, W. Shao, S. Dai, Investigation of precipitation behavior and related hardening in AA 7055 aluminum alloy, Mater. Sci. Eng., A 500 (2009) 34–42, https://doi.org/10.1016/j.msea.2008.09.065.

[35] T.R. Bieler, A.K. Mukherjee, The high strain rate superplastic deformation mechanisms of mechanically alloyed aluminum IN90211, Mater. Sci. Eng., A 128 (1990) 171–182, https://doi.org/10.1016/0921-5093(90)90225-R.

[36] M. Chen, G. Fan, Z. Tan, D. Xiong, Q. Guo, Y. Su, J. Zhang, Z. Li, M. Naito, D. Zhang, Design of an efficient flake powder metallurgy route to fabricate CNT/6061Al composites, Mater. Des. 142 (2018) 288–296, https://doi.org/10.1016/j.matdes.2018.01.044.

[37] R. Xu, Z. Tan, D. Xiong, G. Fan, Q. Guo, J. Zhang, Y. Su, Z. Li, D. Zhang, Balanced strength and ductility in CNT/Al composites achieved by flake powder metallurgy via shift-speed ball milling, Composites Part A 96 (2017) 57–66, https://doi.org/10.1016/j.compositesa.2017.02.017.

[38] Z.Y. Liu, S.J. Xu, B.L. Xiao, P. Xue, W.G. Wang, Z.Y. Ma, Effect of ball-milling time on mechanical properties of carbon nanotubes reinforced aluminum matrix composites, Composites Part A 43 (2012) 2161–2168, https://doi.org/10.1016/j.compositesa.2012.07.026.

[39] F. Wang, B. Xiong, Y. Zhang, H. Liu, X. He, Microstructural development of spray-deposited Al–Zn–Mg–Cu alloy during subsequent processing, J. Alloys Compd. 477 (2009) 616–621, https://doi.org/10.1016/j.jallcom.2008.10.115.

[40] X. Fan, D. Jiang, Q. Meng, L. Zhong, The microstructural evolution of an Al–Zn–Mg–Cu alloy during homogenization, Mater. Lett. 60 (2006) 1475–1479, https://doi.org/10.1016/j.matlet.2005.11.049.

[41] Y. Ii, P. Li, G. Zhao, X. Liu, J. Cui, The constituents in Al–10Zn–2.5Mg–2.5Cu aluminum alloy, Mater. Sci. Eng., A 397 (2005) 204–208, https://doi.org/10.1016/j.msea.2005.02.013.

[42] Z. Li, B. Xiong, Y. Zhang, B. Zhu, F. Wang, H. Liu, Investigation on strength, toughness and microstructure of an Al–Zn–Mg–Cu alloy pre-stretched thick plates in various ageing tempers, J. Mater. Process. Technol. 209 (2009) 2021–2027, https://doi.org/10.1016/j.jmatprotec.2008.04.052.

[43] L.W. Yang, J.Y. Cheng, T. Luoh, P.L. Sun, P.W. Kao, High strain rate superplasticity of a MA Al–8wt%Ti alloy, Scripta Mater. 51 (2004) 47–51, https://doi.org/10.1016/j.scriptamat.2004.03.019.

[44] T.R. Bieler, A.K. Mukherjee, Superplastic deformation mechanisms of mechanical alloyed aluminum, Mater. Trans. 32 (1991) 1149–1158, https://doi.org/10.2320/matertrans1989.32.1149.

[45] S.D. Wu, Theory of Metal Superplastic Deformation, first ed., Nation Defense Industry Press, Beijing, 1997.

[46] Y. Li, T.G. Langdon, A unified interpretation of threshold stresses in the creep and high strain rate superplasticity of metal matrix composites, Acta Mater. 47 (1999) 3395–3403, https://doi.org/10.1016/S1359-6454(99)00219-0.

[47] L. Han, J. Niu, H. Hu, D.O. Northwood, Study on high strain rate superplasticity of a 6061Al alloy composite reinforced with 30 vol.% AlN particulate, J. Mater. Eng. Perform. 13 (2004) 200–207, https://doi.org/10.1361/10599490418415.

[48] M. Mabuchi, K. Higashi, Activation energy for superplastic flow in aluminum matrix composites exhibiting high-strain-rate superplasticity, Scripta Mater. 34 (1996) 1893–1897, https://doi.org/10.1016/1359-6462(96)00069-3.

[49] R.S. Mishra, A.K. Mukherjee, On superplasticity in silicon carbide reinforced aluminum composites, Scripta Mater. 25 (1991) 271–275, https://doi.org/10.1016/0956-716X(91)90177-3.

[50] Y. Li, T.G. Langdon, High strain rate superplasticity in metal matrix composites: the role of load transfer, Acta Mater. 46 (1998) 3937–3948, https://doi.org/10.1016/S1359-6454(98)00073-1.

[51] R. Kaibyshev, T. Sakai, F. Musin, I. Nikulin, H. Miura, Superplastic behavior of a 7055 aluminum alloy, Scripta Mater. 45 (2001) 1373–1380, https://doi.org/10.1016/S1359-6462(01)01172-1.

[52] I. Nikulin, R. Kaibyshev, T. Sakai, Superplasticity in a 7055 aluminum alloy processed by ECAE and subsequent isothermal rolling, Mater. Sci. Eng., A 407 (2005) 62–70, https://doi.org/10.1016/j.msea.2005.06.014.

[53] O.D. Sherby, J. Weertman, Diffusion-controlled dislocation creep: a defense, Acta Mater. 27 (1979) 387–400, https://doi.org/10.1016/0001-6160(79)90031-2.